Scaling relation between the reduction potential of copper catalysts and the turnover frequency for the oxygen and hydrogen peroxide reduction reactions

Langerman, M.; Langevelde, P.H. van; Vijver, J.J. van de; Siegler, M.A., Hetterscheid, D.G.H.

Inorganic Chemistry

pubs.acs.org/IC
Article

Scaling Relation between the Reduction Potential of Copper Catalysts and the Turnover Frequency for the Oxygen and Hydrogen Peroxide Reduction Reactions

Michiel Langerman, Phebe H. van Langevelde, Johannes J. van de Vijver, Maxime A. Siegler, and Dennis G. H. Hetterscheid*

Cite This: *Inorg. Chem.* 2023, 62, 19593−19602
Read Online

ABSTRACT: Changes in the electronic structure of copper complexes can have a remarkable impact on the catalytic rates, selectivity, and overpotential of electrocatalytic reactions. We have investigated the effect of the half-wave potential ($E_{1/2}$) of the Cu^{II}/Cu^{I} redox couples of four copper complexes with different pyridylalkylamine ligands. A linear relationship was found between $E_{1/2}$ of the catalysts and the logarithm of the maximum rate constant of the reduction of O_2 and H_2O_2. Computed binding constants of the binding of O_2 to Cu^{I}, which is the rate-determining step of the oxygen reduction reaction, also correlate with $E_{1/2}$. Higher catalytic rates were found for catalysts with more negative $E_{1/2}$ values, while catalytic reactions with lower overpotentials were found for complexes with more positive $E_{1/2}$ values. The reduction of O_2 is more strongly affected by the $E_{1/2}$ than the H_2O_2 rates, resulting in that the faster catalysts are prone to accumulate peroxide, while the catalysts operating with a low overpotential are set up to accommodate the 4-electron reduction to water. This work shows that the $E_{1/2}$ is an important descriptor in copper-mediated O_2 reduction and that producing hydrogen peroxide selectively close to its equilibrium potential at 0.68 V vs reversible hydrogen electrode (RHE) may not be easy.

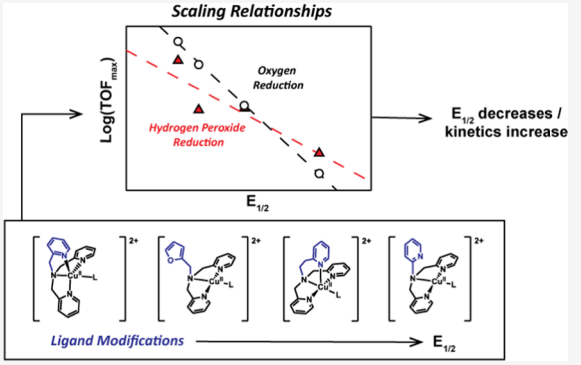

INTRODUCTION

The electrochemical oxygen reduction reaction (ORR) can either result in the 4-electron reaction product (H_2O) or the 2-electron reaction product (H_2O_2), both involving different standard equilibrium potentials for the respective reactions involved, as shown in Scheme 1. Additionally, the 4-electron pathway may proceed via H_2O_2 as an intermediate as a result of two consecutive $2H^+/2e^-$ reaction steps. Both the 4-electron reduction of dioxygen (O_2) to water and 2-electron reduction to H_2O_2 are important reactions in relation to their application in fuel cell technology and the use of H_2O_2 as a powerful oxidant and potential energy carrier.[1−7]

Inspired by enzymes such as copper-based monooxygenases and oxidases, the chemistry of copper complexes with O_2 has been widely explored.[8−12] Many potential catalytic intermediates have been spectroscopically identified, or even isolated, and their reactivity toward various reactants has been thoroughly studied by the bioinorganic chemistry community.[13−17] A smaller amount of copper complexes have been successfully studied for the electrochemical reduction of dioxygen, in which some of the more elegant studies showed a good correlation between biology, bioinorganic model systems, and electrochemical behavior.[18] However, many of the studies directed toward the ORR output have been carried out with less well-defined heterogenized and amorphous samples,[19,20] and clear design principles regarding fast and selective copper-based electrocatalysts for the ORR have not yet been established.[21]

Recently, we showed that the tetradentate copper complex $[Cu(tmpa)(L)]^{2+}$ (Cu-tmpa) (tmpa = tris(2-pyridylmethyl)-amine), (L = solvent), has very high reaction rates for the electrochemical ORR.[22−24] It was shown that a full reduction of dioxygen to water takes place via a stepwise process with H_2O_2 as a detectable intermediate. Both the partial reduction of O_2 to water and the reduction of H_2O_2 catalyzed by Cu-tmpa demonstrated high catalytic rate constants, with only a small difference in onset potential between the 2-electron ORR and the hydrogen peroxide reduction reaction (HPRR).[22,23] This resulted in a small potential window, where H_2O_2 is the primary product during catalysis. Additionally, the fast catalytic

Received: August 23, 2023
Revised: October 26, 2023
Accepted: November 6, 2023
Published: November 17, 2023

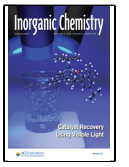

https://doi.org/10.1021/acs.inorgchem.3c02939
Inorg. Chem. 2023, 62, 19593−19602

Scheme 1. Standard Electrode Potentials of the Different Catalytic Reactions Involved in the ORR, and Postulated Mechanism for the ORR and Hydrogen Peroxide Reduction Reaction (HPRR) Mediated by Cu-tmpa

$O_2 + 4H^+ + 4e^- \rightleftharpoons 2H_2O$ $E^0 = 1.23$ V vs. RHE

$O_2 + 2H^+ + 2e^- \rightleftharpoons H_2O_2$ $E^0 = 0.695$ V vs. RHE

$H_2O_2 + 2H^+ + 2e^- \rightleftharpoons 2H_2O$ $E^0 = 1.78\ V\ vs.\ RHE$

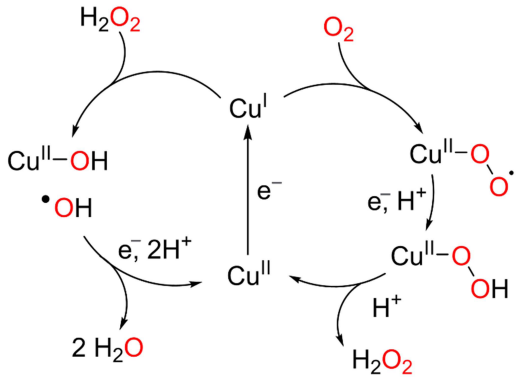

rates for both reactions come at the cost of a significant overpotential. In order to reduce the overpotential and steer the selectivity toward either the full 4-electron or 2-electron reduction of dioxygen, a better fundamental understanding is necessary between the (electronic) structure of the copper catalyst and the catalytic activity for the ORR and HPRR.

While a correlation between the catalytic ORR activity and the electronic structure of these Cu complexes has not been addressed in any form, the effect of ligand denticity and flexibility on the geometry and electronic structure of copper complexes has been a subject of intense study.[25−33] A significant library of different ligand modifications has been investigated for copper complexes based on the tetradentate pyridine ligand scaffold of Cu-tmpa.[34−36] In light of structure−activity correlations in Cu-catalyzed ORR, the half-wave potential ($E_{1/2}$) is a particularly interesting parameter, given that the reduction of Cu from the +II to the +I oxidation state is potential-determining for the more competent catalytic systems.[22] We have therefore selected a number of catalysts (Scheme 2) from the literature and some of our own previously unpublished work to investigate the relationship between $E_{1/2}$ and the catalytic performance in the ORR and HPRR by employing voltammetry, rotating ring-disk experiments, and density functional theory (DFT) calculations.

RESULTS AND DISCUSSION

Selection of Catalysts. In addition to the previously reported Cu-tmpa system,[22,23] we selected three different mononuclear copper complexes, as shown in Scheme 2. In two of these, $[Cu(pmea)(L)]^{2+}$ (Cu-pmea; pmea = bis[(2-pyridyl)methyl]-2-(2-pyridyl)ethylamine) and $[Cu(bpmpa)(L)]^{2+}$ (Cu-bpmpa; bpmpa = bis[(2-pyridyl)methyl]-2-pyridylamine), the distance between the central tertiary amine and one of the pyridine arms was varied by changing methylene to an ethylene spacer (Cu-pmea) or removing it altogether, resulting in an aminopyridine moiety (Cu-bpmpa). A crystal structure of $[Cu(bpmpa)(Cl)]ClO_4$ shows that the pyridine N of the aminopyridine does not coordinate with the copper center.[28] This noncoordinated pyridine moiety could interact with protons present in intermediate species during the ORR and HPRR reactions. Proton shuttles in the second coordination sphere have led to a significant increase in turnover frequency (TOF) for many catalytic systems.[37,38] Given that no H^+ transfer is involved in the rate-determining step of the Cu-mediated ORR, we do not anticipate a significant effect on the catalytic rate here.[22,23] The third complex, $[Cu(fubmpa)(H_2O)(OTf)_2]$ (Cu-fubmpa; fubmpa = *N*-(furan-2-ylmethyl)-*N*-[bis(2-pyridyl)methyl]amine), was designed as an analogue of the copper complex $[Cu(bmpa)(L)]^{2+}$ (bmpa = bis(2-pyridylmethyl)amine),[39] by introduction of the noncoordinating furanyl moiety while maintaining the nature of the central tertiary amine. We have selected these complexes because their $E_{1/2}$ values range between 0.2 and 0.5 V vs reversible hydrogen electrode (RHE), and, as far as we could observe, no limitations in electron transfer rates occurred within this selected series of tmpa modifications (see below), as opposed to our previous observations in the case of rigid terpyridine catalysts.[39]

Synthesis. The polypyridyl ligands bis[(2-pyridyl)methyl]-2-(2-pyridyl)ethylamine (pmea) and bis[(2-pyridyl)methyl]-2-pyridylamine (bpmpa) have been previously reported and were synthesized in a one-step reaction via reductive amination and nucleophilic substitution (S_N2), respectively.[28,40] The ligand *N*-(furan-2-ylmethyl)-*N*-[bis(2-pyridyl)methyl]amine (fubmpa) was synthesized from commercially available furan-2-ylmethanamine and 2-pyridinecarboxaldehyde via a reductive amination in a one-step reaction. Following purification by column chromatography, fubmpa was characterized by ^{1}H NMR, ^{13}C NMR, and electrospray ionization mass spectrometry (ESI MS). The copper complexes, $[Cu(pmea)(CH_3CN)](OTf)_2$ and $[Cu(bpmpa)(CH_3CN)](OTf)_2$, were synthesized by mixing the respective ligand with $Cu(OTf)_2$ in a 1:1 ratio in dry CH_3CN under an inert atmosphere, and characterization was performed by ESI MS and elemental analysis (see the

Scheme 2. Overview of the Structures of the Three Different Copper(II) Complexes Investigated in This Work in Addition to Cu-tmpa

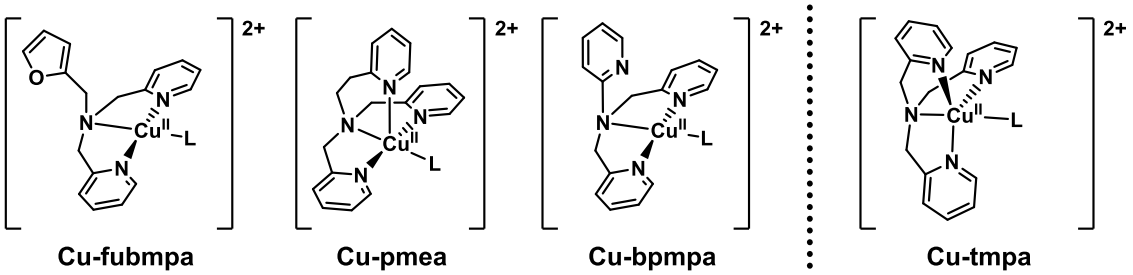

https://doi.org/10.1021/acs.inorgchem.3c02939
Inorg. Chem. 2023, 62, 19593−19602

Experimental Section). The copper complex [Cu(fubmpa)-$(H_2O)(OTf)_2$] was synthesized by mixing fubmpa with $Cu(OTf)_2$ in a 1:1 ratio in CH_3CN. The resulting complex was purified by crystallizing the complex twice from CH_3CN by the addition of diethyl ether. Characterization of Cu-fubmpa was done by elemental analysis, single-crystal X-ray crystallography, and UV−vis spectroscopy. The single crystals suitable for X-ray structure determination were obtained via liquid−liquid diffusion in an NMR tube, with Cu-fubmpa dissolved in chloroform and layered with diethyl ether. A projection of the structure is shown in Figure 1. In the crystal

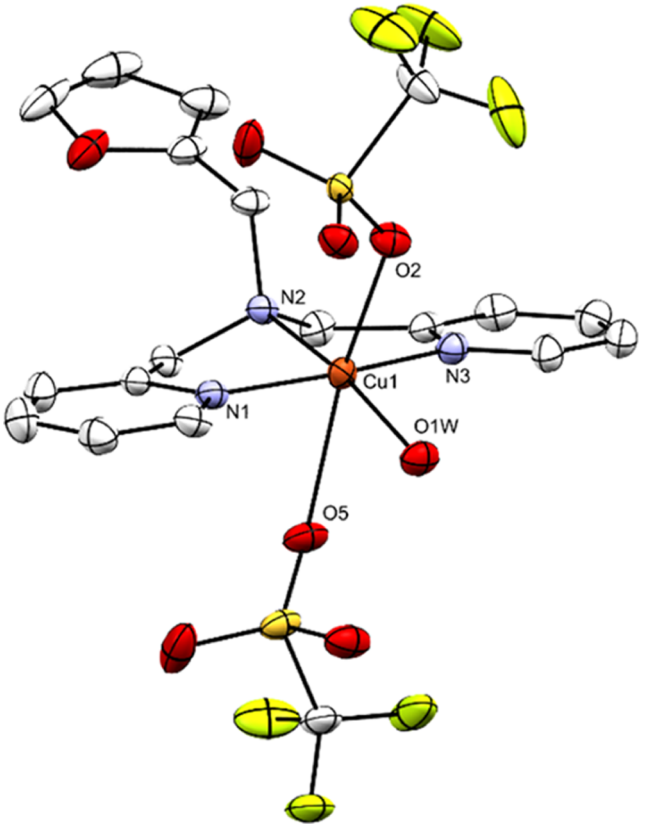

Figure 1. Displacement ellipsoid plot (50% probability level) of Cu-fubmpa at 110(2) K. The H atoms, disorder, and lattice water solvent molecules are omitted for clarity. Hydrogen bond interactions of O1W with several lattice water solvent molecules are shown in Figure S7.

structure, the top axial OTf^- ligand has a Cu−O bond distance of 2.3749(15) Å. However, the Cu1−O5 distance between the copper center and the second triflate is 2.6646(16) Å. This is on the long side for an axial Cu−O bond and points to a more square pyramidal coordination environment rather than an octahedral geometry.[41−44] Both elemental analysis and single-crystal X-ray crystallography show that a water molecule is coordinated to the copper center, likely originating from the $Cu(OTf)_2$ salt, which has a tendency to form hydrates when exposed to air. The coordinated water molecule forms two O−H···O hydrogen bonds (1.980 Å) with one of the oxygen atoms of the axial triflate ligand below the plane and one lattice water solvent molecule. Additionally, the crystal structure confirms that the furanyl group does not coordinate to the Cu center. UV−vis spectra were measured in Milli-Q water, and the extinction coefficient (ε) for the d−d transition at 660 nm is 1.0×10^2 L mol^{-1} cm^{-1}, and for the absorption peak at 251 nm, an ε of 9.7×10^3 L mol^{-1} cm^{-1} was found (Supporting Information, Section S2).

Electrochemistry of Cu-fubmpa, Cu-bpmpa, and Cu-pmea. To study the effect of the different ligands on the redox chemistry of the complexes, cyclic voltammograms (CVs) of the complexes in a pH 7 phosphate buffer (PB) solution under an argon atmosphere were recorded using a glassy carbon (GC) working electrode (A = 0.0707 cm^2). The resulting redox couples recorded of Cu-fubmpa, Cu-bpmpa, and Cu-pmea with a scan rate of 100 mV s^{-1} are combined in Figure 2,

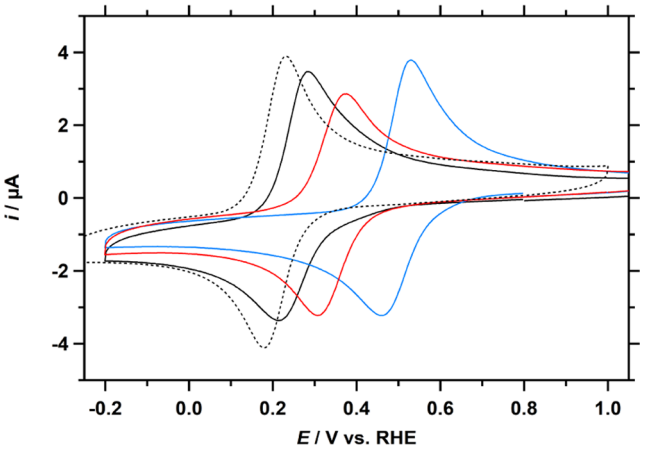

Figure 2. Cyclic voltammograms of Cu-fubmpa (black), Cu-pmea (red), and Cu-bpmpa (blue), including Cu-tmpa (dotted) as a reference, in a pH 7 phosphate buffer under 1 atm Ar. For each copper complex, a concentration of 0.3 mM was used. Conditions: pH 7 PB ($[PO_4]$ = 100 mM), 293 K, 100 mV s^{-1} scan rate.

with Cu-tmpa as the reference complex. The $E_{1/2}$ of the $Cu^{II/I}$ redox couples of these complexes span a wide potential range (Table 1), shifting positively from the $E_{1/2}$ of 0.21 V for Cu-tmpa to 0.25 V for Cu-fubmpa, 0.37 V for Cu-pmea, and 0.49 V for Cu-bpmpa. All three complexes show lower peak currents (i_p) than Cu-tmpa for both the cathodic (i_{pc}) and anodic (i_{pa}) peaks, resulting in slightly lower diffusion coefficients (see Table 1 and Supporting Information, Section S4).

Electrocatalytic Performance toward the ORR and HPRR. We have previously shown that Cu-tmpa produces H_2O_2 as a detectable intermediate during the electrocatalytic reduction of O_2, but it can also further reduce H_2O_2 to H_2O.[22,23] In line with these findings, both the ORR and HPRR were studied for Cu-fubmpa, Cu-bpmpa, and Cu-pmea. CVs were measured in a pH 7 phosphate buffer solution containing 0.3 mM of the complex under 1 atm O_2 or with 1.1 mM H_2O_2 under 1 atm Ar. The resulting catalytic waves for the reduction of O_2 and H_2O_2 are shown in Figure 3 separately for each catalyst. One observation that can immediately be made is that the ORR current is greater than the HPRR current for all of the analyzed complexes. This was also observed for Cu-tmpa previously and most likely related to mass transport limitations in O_2 and H_2O_2. Our experiments are set up such that the local concentrations of O_2 and H_2O_2 are similar (1.2 mM), yet the diffusion coefficient of O_2 (1.9×10^{-5} cm^2 s^{-1}) is significantly larger than that of H_2O_2 ($0.8-1.4 \times 10^{-5}$ cm^2 s^{-1}).[45,46] Moreover, the HPRR is a 2-electron process, while the ORR may consume up to 4 electrons, particularly under mass

https://doi.org/10.1021/acs.inorgchem.3c02939
Inorg. Chem. 2023, 62, 19593−19602

Table 1. TOF_{max} for the ORR and HPRR Derived from Foot-of-the-Wave Analysis (FOWA)

complex	redox couple		TOF_{max} (s^{-1})	
	$E_{1/2}$ (V)	D (cm^2 s^{-1})[b]	ORR	HPRR
Cu-tmpa[a]	0.206	4.9×10^{-6}	$1.8 \times 10^6 \pm 0.6 \times 10^6$	$2.1 \times 10^5 \pm 0.1 \times 10^5$
Cu-fubmpa	0.248(2)	2.4×10^{-6}	$1.3 \times 10^5 \pm 0.3 \times 10^5$	$0.8 \times 10^3 \pm 0.1 \times 10^3$
Cu-pmea	0.341(2)	2.9×10^{-6}	$1.4 \times 10^3 \pm 0.2 \times 10^3$	$1.0 \times 10^3 \pm 0.3 \times 10^3$
Cu-bpmpa	0.494(2)	2.3×10^{-6}	0.7 ± 0.06	6.4 ± 0.9

[a]Data from refs 22 and 23. [b]Determined from Randles–Sevcik analysis of i_{pc}. conditions: 0.3 mM catalyst concentration, pH 7 PB ($[PO_4]$ = 100 mM), 293 K, 100 mV s^{-1} scan rate, 0.0707 cm^2 electrode surface area.

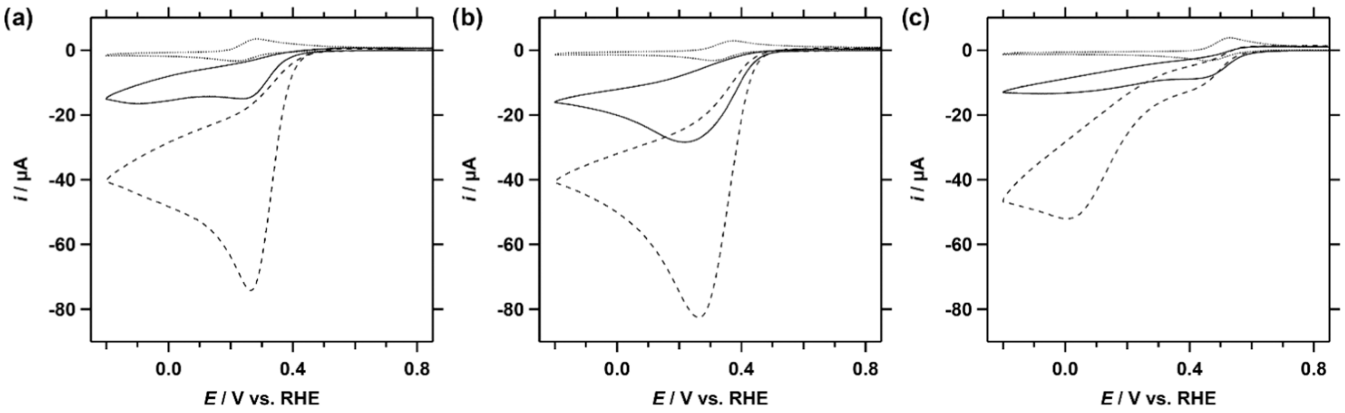

Figure 3. CVs of Cu-fubmpa (a), Cu-pmea (b), and Cu-bpmpa (c) in a PB pH 7 electrolyte solution under 1 atm Ar (dotted line), 1 atm O_2 (dashed line), or with 1.1 mM H_2O_2 under 1 atm Ar (solid line). For each catalyst, a concentration of 0.3 mM was used. Conditions: pH 7 PB ($[PO_4]$ = 100 mM), 293 K, 100 mV s^{-1} scan rate, 0.0707 cm^2 electrode surface area.

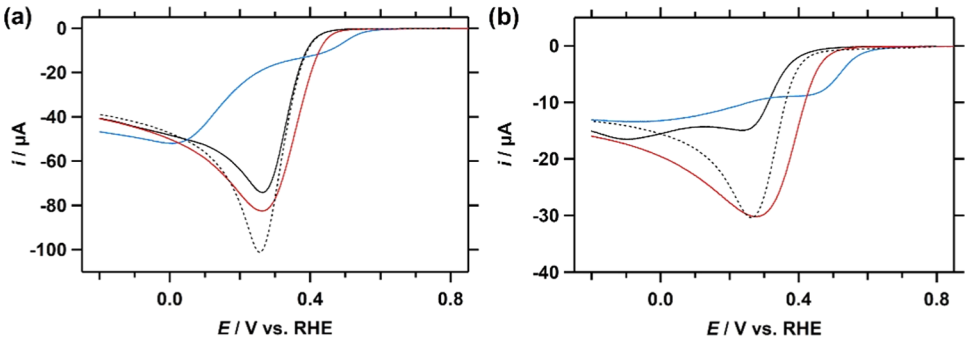

Figure 4. Linear sweep voltammograms (LSV) of Cu-fubmpa (black), Cu-pmea (red), and Cu- bpmpa (blue), including Cu-tmpa (dotted) as a reference, under 1 atm O_2 (a), or in the presence of 1.1 mM H_2O_2 under 1 atm Ar (b). For each catalyst, a concentration of 0.3 mM was used. Conditions: pH 7 PB ($[PO_4]$ = 100 mM), 293 K, 100 mV s^{-1} scan rate, 0.0707 cm^2 electrode surface area.

transport-limited conditions. For Cu-fubmpa, the onset of the ORR appears to be ca. 40 mV higher compared with the onset of the HPRR (Figure S19). Here, the onset is defined as $i_{cat}/i_p \geq 2$ (see the Supporting Information, Table S4). On the other hand, both Cu-bpmpa and Cu-pmea each show overlapping catalytic onsets for the ORR and HPRR. The HPRR onset for Cu-fubmpa is shifted to a lower potential, something that was also observed for Cu-tmpa.[23]

The catalytic linear sweep voltammograms (LSVs) of Cu-fubmpa, Cu-bpmpa, and Cu-pmea complexes of the ORR and HPRR are combined in Figure 4 to allow for a straightforward comparison between the catalysts. The catalytic wave of the ORR in the presence of Cu-fubmpa overlaps neatly with the catalytic wave of Cu-tmpa, while the catalytic onset potential of Cu-pmea is slightly higher. However, both catalysts reach a somewhat lower peak catalytic current (i_{cat}) than Cu-tmpa. Cu-bpmpa, on the other hand, shows a much earlier onset than the other catalysts, nearer to the 0.695 V vs RHE equilibrium potential of the O_2/H_2O_2 couple. However, a tradeoff for this higher onset potential is the much lower catalytic activity exhibited by the catalyst. In addition, further reduction of the catalytic site appears required before satisfactory reaction rates can be observed (Section S5).

The voltammetry data from the HPRR show a similar trend for the onset potential of the catalytic reaction, with the onset in the presence of Cu-fubmpa < Cu-pmea < Cu-bpmpa (Figure 4b). Of the three catalysts investigated here, fairly similar catalytic currents are observed for Cu-pmea and Cu-tmpa, which is most likely the result of mass transport limitations rather than a true catalytic effect. A lower slope and thus a smaller increase in catalytic rate as a function of applied potential hints at a lower HPRR rate constant for Cu-pmea. The catalytic current of Cu-fubmpa is again significantly lower.

Correlation between $E_{1/2}$ and the Catalytic Rates of ORR and HPRR Using the Foot-of-the-Wave Analysis. The electrochemical reduction of O_2 proceeds via H_2O_2 as an

https://doi.org/10.1021/acs.inorgchem.3c02939
Inorg. Chem. 2023, 62, 19593−19602

obligatory intermediate in the case of Cu-tmpa[22] and related pyridylalkylamine complexes.[39,47,48] Therefore, the electron transfer number is 2 at the foot-of-the-wave, while the electron transfer number is ill-defined at the peak-of-the-wave, where over-reduction to water is likely to occur. We therefore rely for determination of the catalytic rates for the ORR and HPRR on the foot-of-the-wave equation (eq 1), which produces more satisfactory results than the current enhancement method (CE, see the Supporting Information, Section S6). The FOWA extrapolates the ideal or maximum turnover frequency (TOF_{max}) of the catalyst from the foot of the catalytic wave, close to the onset of the catalytic reaction (an elaborate detailed description of FOWA was recently given by Dempsey et al.).[49] An additional advantage of the FOWA method over CE is that it avoids side phenomena, such as O_2 depletion, which occurs readily due to the limited O_2 concentration of roughly 1.2 mM at room temperature (293 K) under atmospheric pressure.[50]

For the FOWA, CVs were measured in triplicate in a PB (pH 7) electrolyte solution containing 0.3 mM complex and 1 atm O_2 (for the ORR), or 1.1 mM H_2O_2 in the presence of 1 atm Ar (for the HPRR), using a freshly polished GC electrode for each measurement (see the Supporting Information, Section 6.2). These voltammograms were used to construct plots of the current enhancement i_c/i_p vs $(1 + \exp[F/RT(E - E_{1/2})])^{-1}$, where i_c is the catalytic current measured in the presence of catalyst and substrate (O_2 or H_2O_2) at the applied potential E and i_p is the peak current of the Cu^{II} reduction in the absence of the substrate. In the foot-of-the-wave potential window, a linear fit was obtained between the catalytic onset and the potential, where i_c/i_p is at least equal to 1.6. The onset is defined as $i_c/i_{redox} \geq 2$, where i_{redox} is the current measured at the applied potential E in the presence of the catalyst but in the absence of the substrate. The TOF_{max} was determined from the slope of the linear fit by applying eq 1. Assumed here is that for fast electrocatalytic reactions, as described here, all electrons necessary to reduce dioxygen (and hydrogen peroxide) come from the electrode and not from neighboring homogeneous sites.[51] In a previous study,[22,23] it was already established that in the case of Cu-tmpa, the potential-determining step is reduction of Cu(II) to Cu(I) and that binding of O_2 to Cu(I) occurs during the rate-determining step in line with a EC′ mechanism.[52] This signifies that eq 1 is the appropriate FOWA equation in the case of Cu-tmpa. Based on the shape of the FOWA plots (see the Supporting Information), we can assume the same type of reaction mechanism across all catalysts.

$$\frac{i_c}{i_p} = \frac{2.24 n_{cat}\sqrt{\frac{RT}{Fv}TOF_{max}}}{1 + \exp\left[\frac{F}{RT}(E - E_{1/2})\right]} \quad (1)$$

The resulting TOF_{max} values for the ORR and HPRR are reported in Table 1. For the ORR, Cu-fubmpa has the highest TOF_{max} (1.3×10^5 s^{-1}), while Cu-bpmpa has the lowest (0.7 s^{-1}). For the HPRR, Cu-pmea shows the highest TOF_{max}, but it is closely followed by Cu-fubmpa. All catalysts discussed here have a TOF_{max} lower than that of the previously reported Cu-tmpa for both catalytic reactions. Comparison of the ORR and HPRR TOF_{max} values reveals an interesting trend. The TOF_{max} of both catalytic reactions decreases with increasing $E_{1/2}$ values of the complexes, which results in a change in the relative magnitude of the TOF_{max} of both reactions (Figure 5). For both reactions, a linear fit through the data points was

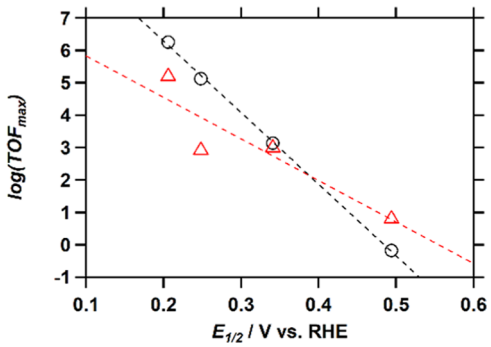

Figure 5. Plot of the logarithm of the TOF_{max} of the ORR (circles; 1 atm O_2) and HPRR (triangles; 1.1 mM H_2O_2) versus the $E_{1/2}$ of the respective catalysts, including Cu-tmpa. Linear fit ORR (black dashed line): $y = -22.1x + 10.7$, $R^2 = 0.99$. Linear fit HPRR (red dashed line): $y = -13.1x + 7.2$, $R^2 = 0.82$.

obtained, resulting in an R^2 value that is close to 1 in the case of the ORR and 0.82 for the HPRR. For Cu-fubmpa, the ORR is much faster than the HPRR, while for Cu-bpmpa, which has the highest $E_{1/2}$, the ORR is slower than the HPRR. For Cu-pmea, both reactions show similar TOF_{max} values. Thus, the higher the $E_{1/2}$, the more the reduction of H_2O_2 seems to be favored over the reduction of O_2. However, the FOWA does not consider the second, higher catalytic wave observed for Cu-bpmpa in the presence of O_2, as the TOF_{max} is derived from the initial slope around 0.6 V vs RHE. This second catalytic wave, which is centered at 0.1 V vs RHE, cannot be accurately probed by the FOWA but shows that higher catalytic rates can be achieved in the presence of Cu-bpmpa. This may either point to the formation of a second catalytic species or to reduction of dioxygen via a different reaction mechanism. Either way, the higher catalytic activity observed in the second catalytic wave is at the cost of a significantly increased overpotential. The TOF_{max} values obtained by FOWA, and k_{obs} values obtained by CE methods compare well in the case of Cu-tmpa and Cu-fubmpa, yet lead to dissimilar results in the case of Cu-pmea and Cu-bpmpa, which seem to be related to further activation of the catalyst beyond the initial onset of the catalytic wave (see Section S6).

O_2 Binding Constant Determination by DFT. Electrochemical methods point to a linear scaling relationship between the $\log(TOF_{max})$ values for the ORR and HPRR and the $E_{1/2}$ of the catalyst. In order to relate the electronic structure of the catalytic intermediates to the redox potential of the catalyst, density functional theory (DFT) calculations on key catalytic species were carried out (Section S9). In this manner, binding energies of O_2 to the Cu(I) state of the catalysts could be obtained. Both the triplet state and broken-symmetry singlet state were obtained for the superoxide state of all complexes. In all cases, the triplet state corresponds to the ground state energy of the complexes. This is in line with earlier reports on copper(II) superoxide complexes with side-on O_2 binding[53] and previously calculated Cu-tmpa superoxide species.[54] As depicted in Figure 6, the obtained O_2 binding energies depend linearly on the $E_{1/2}$ since the more electron-rich copper sites tend to bind O_2 more strongly. In addition, the binding energies of O_2 to the water adducts of Cu-fubmpa ($[Cu(fubmpa)H_2O]^+$) and Cu-bpmpa ($[Cu(bpmpa)H_2O]^+$) were calculated as their tridentate ligands might provide an extra coordination site for water compared to the tetradentate ligands. These binding energies were excluded from the linear

https://doi.org/10.1021/acs.inorgchem.3c02939
Inorg. Chem. 2023, 62, 19593−19602

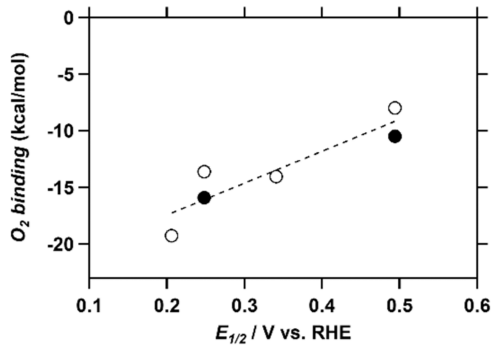

Figure 6. Plot of the calculated binding energies of O_2 to the Cu(I) state of $[Cu(tmpa)]^+$ ($E_{1/2}$ = 0.206), $[Cu(fubmpa)]^+$ ($E_{1/2}$ = 0.248), $[Cu(fubmpa)H_2O]^+$ ($E_{1/2}$ = 0.248), $[Cu(pmea)]^+$, $[Cu(bpmpa)]^+$ ($E_{1/2}$ = 0.494), and $[Cu(bpmpa)H_2O]^+$ ($E_{1/2}$ = 0.494) versus the $E_{1/2}$ of the respective catalysts. For Cu-fubmpa and Cu-bpmpa, the two data points represent the complexes with (solid circle) and without (open circle) a molecule of water coordinated to the copper site. The linear fit was fitted through the data points that represent the complexes without additional water (open circles), with R^2 = 0.84.

fit but followed the same trend. Previously, it was found that the RDS for the ORR by Cu-tmpa is most probably the binding of O_2.[22] Based on the trends displayed in Figure 5, this hypothesis can be further extended to Cu-fubmpa, Cu-pmea, and Cu-bpmpa, as both O_2 binding and TOF_{max} now scale with $E_{1/2}$. Therefore, this finding provides a rationale for the reaction rate, which thus depends on the binding energy of O_2, which is determined by the $E_{1/2}$.

Regarding the binding of H_2O_2 to the Cu(I) states of all catalysts, the differences in binding energies are small and fall within the error range of the computations (see Section S9). In line with our previously published results, H_2O_2 binding probably occurs in a pre-equilibrium, while the rate-determining step of HPRR is probably associated with O−O bond scission.[9−23]

Rotating Ring-Disk Electrode Measurements. Interestingly, Figure 5 shows that at a certain $E_{1/2}$ value, the relative activities for the ORR and HPRR invert, resulting in the HPRR becoming the faster catalytic reaction of the two as the $E_{1/2}$ of the catalyst increases. This implies that the $E_{1/2}$ of the Cu complex must be a key descriptor regarding the selectivity of the ORR and generation of H_2O_2 mediated at single-site copper species. To investigate this hypothesis, rotating ring-disk electrode (RRDE) measurements were performed. These measurements allow us to determine the selectivity of all catalysts for the overall 2- vs 4-electron reduction of oxygen, as the hydrogen peroxide that is generated at the disk can be detected and quantified at a Pt ring. RRDE measurements of Cu-pmea, Cu-bpmpa, and Cu-fubmpa were recorded and compared to the previously reported RRDE data of Cu-tmpa.[22,23] LSV measurements in 0.1 M PB show for Cu-fubmpa and Cu-pmea a catalytic current that reaches a limiting plateau current below 0.2 V vs RHE. In the case of Cu-bpmpa, a plateau current is not reached; instead, the LSV shows a small catalytic wave, followed by a second larger catalytic wave at a much lower potential (Figure S21), which is in line with the CV data from Figure 3c. Analysis of the catalytic currents at different rotation rates shows for all catalysts that the current linearly depends on the square root of the rotation, indicating that the number of electrons transferred does not depend on rotation speed (see Figure S23). In addition, the onset potential of the catalytic ORR was determined in the same manner for stationary CV experiments and followed the same trend (Figure S24 and Table S4).

Subsequently, analysis of the current measured at the Pt ring allows us to determine the selectivity of the catalysts during catalysis of the ORR and verifies that H_2O_2 is produced as an (intermediate) product (see Figure S25). Figure 7a,b shows the selectivity of the ORR determined from the LSV and chronoamperometry (CA) experiments for all four catalysts. In general, the LSV and CA data follow the same trends, but there is a deviation between the exact values, caused by the different nature of both experiments. To make sure that the H_2O_2 selectivity is determined correctly, the reproducibility of both measurements was verified (see Figure S21). Besides the selectivity, the catalytic current that is used to convert oxygen to hydrogen peroxide ($i_{H_2O_2}$) can be determined from RRDE measurements as well, as shown in Figure 7c. The trends on H_2O_2 selectivity and $i_{H_2O_2}$ for the different catalysts can be explained with the help of Figure 7d, in which the TOF_{max} of the ORR is plotted vs the TOF_{max} of the HPRR, as determined by FOWA (see Table 1). This graph indicates to what extent one of these two reactions proceeds faster. In general, for the ORR > HPRR regime, the TOF_{max} of the ORR is higher than that of the HPRR and H_2O_2 is generated faster than it can be consumed, while for the HPRR > ORR regime, the opposite is true. On top of this, it is important to note that for faster catalysts, the consumption of the substrate, both O_2 and H_2O_2, will be quicker. As a consequence, faster catalysts will quickly consume O_2, which will result in over-reduction of H_2O_2 to H_2O, at the cost of a lower H_2O_2 selectivity. We can now rationalize the trends in selectivity and $i_{H_2O_2}$ in Figure 7 by considering the relative rates of the ORR and HPRR in Figure 7d.

Starting from the catalyst with the highest $E_{1/2}$, Cu-bpmpa is not much more active than the bare GC electrode, especially at the start of the catalytic wave. The small quantities of H_2O_2 detected at the ring may in part originate from the bare GC electrode, which makes the interpretation of the data difficult. Only at potentials below 0.0 V vs RHE, the catalyst is clearly more active than the GC electrode and the H_2O_2 selectivity of Cu-bpmpa instantly starts to drop (see Figure S22). The small $i_{H_2O_2}$ and low H_2O_2 selectivity are expected, as this catalyst is slowest for both ORR and HPRR, with the HPRR rate being higher than the ORR rate. Next, Cu-pmea is a more active catalyst for both the ORR and HPRR compared to Cu-bpmpa, resulting in a larger $i_{H_2O_2}$. This catalyst produces H_2O_2 close to the onset of the ORR, but both selectivity to H_2O_2 and $i_{H_2O_2}$ drop at lower potentials. This can be explained by the HPRR rate being close to the ORR rate. The TOF_{max} of the HPRR for Cu-pmea is comparable to that of Cu-fubmpa. However, for Cu-fubmpa, the rate of the ORR is much higher than that of the HPRR. This results in a high selectivity to H_2O_2 and a large $i_{H_2O_2}$ over the whole potential window compared to the other catalysts. Lastly, for Cu-tmpa, the ORR rate is higher than the HPRR at the same substrate concentrations. In addition, the rates for both ORR and HPRR are much faster compared to the other catalysts. As a result, Cu-tmpa will quickly convert most O_2 to H_2O_2, while, in turn, this H_2O_2 is also quickly consumed to generate H_2O, as shown previously.[22,23] This results in a H_2O_2 selectivity that is, in general, lower than that for Cu-fubmpa. Taken together, we can explain the RRDE

https://doi.org/10.1021/acs.inorgchem.3c02939
Inorg. Chem. 2023, 62, 19593−19602

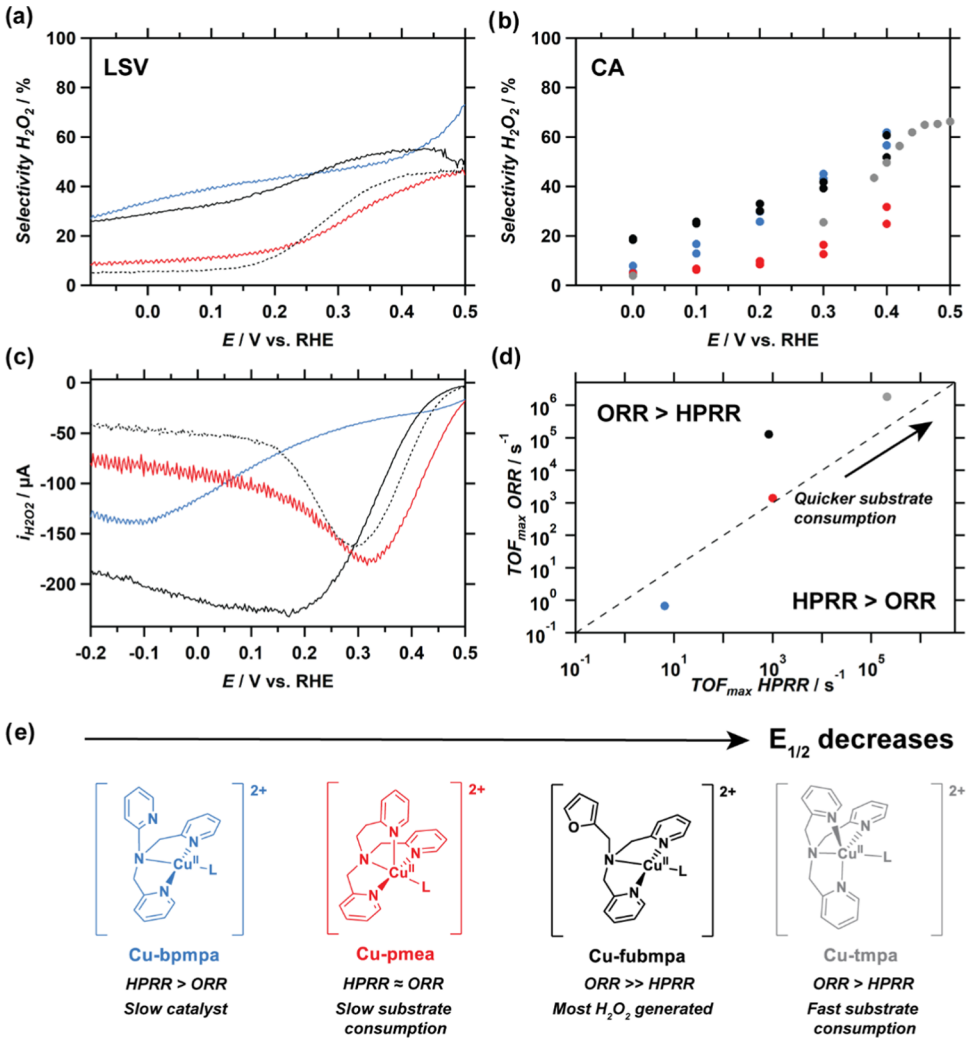

Figure 7. Selectivity of the ORR determined from RRDE LSV (a) and CA (b) experiments and catalytic current to H_2O_2 (2-electron ORR) determined from RRDE LSV data (c) catalyzed by Cu-fubmpa (black), Cu-bpmpa (blue), Cu-pmea (red), and Cu(tmpa) (gray dots/dotted line) under 1 atm O_2. (d) Compared to a plot of the TOF_{max} values determined for ORR and HPRR for Cu-fubmpa (black), Cu-bpmpa (blue), Cu-pmea (red), and Cu(tmpa) (gray) as shown in Table 1. Data for Cu-tmpa obtained from ref 22. Catalyst structures and the most important conclusions are shown in panel (e). A catalyst concentration of 0.3 mM was used for each complex. Conditions: pH 7 PB ($[PO_4]$ = 100 mM), 293 K, 0.196 cm^2 electrode surface area, 1600 RPM, Pt ring at 1.2 V vs RHE.

results in terms of product selectivity and $i_{H_2O_2}$ based on the TOF_{max} of the ORR and HPRR, which are in turn linked to the $E_{1/2}$ of these catalysts. From the RRDE data, the most H_2O_2 is generated in the case of Cu-fubmpa, which has a relatively high ORR rate compared to the HPRR. In turn, 4-electron reduction of oxygen can either be achieved by a catalyst that has a similar TOF_{max} for the HPRR and ORR, as is the case for Cu-pmea, or by a catalyst that will quickly consume all O_2, ultimately leading to further reduction of H_2O_2 to H_2O, which is the case for Cu-tmpa.

DISCUSSION

Variation in the length of the $(-CH_2)_n$ spacer (where n = 0−2) between the central tertiary amine and one of the pyridine moieties results in a significant shift in the equilibrium potential of the Cu^{II}/Cu^{I} redox couple. These observations are fully in line with the results of the Rorabacher and Karlin groups in the past, who have shown a clear correlation between the ligand-ring size and the Cu^{II}/Cu^{I} redox couple.[26,27,55,56] The shifts of Cu-pmea and Cu-bpmpa toward a higher potential are much larger than observed for Cu-fubmpa, in which one of the pyridine arms is replaced for a furanyl group, thereby keeping the central tertiary amine intact while preventing the coordination of a third ligand arm to the Cu center. In this way, the effect of a lower denticity on the catalytic activity could be investigated without removing the pyridine arm entirely, as this would have introduced a secondary amine that could be easily oxidized during the catalytic cycle. Indeed, the $E_{1/2}$ of Cu-fubmpa and Cu-bmpa (bmpa = bis(2-pyridylmethyl)amine) is similar in a pH 7 phosphate buffer (the $E_{1/2}$ of Cu-bmpa is 0.30 V vs RHE),[39] indicating that the coordination of the furanyl group does not occur while in solution.

A linear relationship between the maximum TOF [log(TOF_{max})] and the $E_{1/2}$ of the catalytic species is observed, as visualized in Figure 5. As the catalyst $E_{1/2}$ increases and thus the overpotential decreases, the rate of the reaction decreases. This behavior seems to hold for both the ORR and the HPRR, although the effect is smaller with more deviations in the case of the HPRR TOF_{max}. Such Evans−Polanyi type scaling

https://doi.org/10.1021/acs.inorgchem.3c02939
Inorg. Chem. 2023, 62, 19593−19602

relations between the log rate and typically the overpotential have been reported previously in the case of some very well-behaved electrocatalysts.[57−61] Typically, these scaling relations are plotted versus the overpotential of the catalytic reaction.[47,58−60] We believe that in this context, the $E_{1/2}$ is a more appropriate descriptor than, for example, the overpotential that is frequently used given that the overpotentials of ORR and HPRR are often ill-defined if these are not fully under a kinetic control. Moreover, the relationship versus $E_{1/2}$ allows for a more facile comparison between the ORR and HPRR results, which have different standard reduction potentials. Not only log TOF_{max} but also the computed binding constant of O_2 to the various copper site correlates well with the $E_{1/2}$ value of these copper sites. These correlations are in perfect agreement with a potential-determining reduction of Cu^{II} to Cu^{I}, followed by rate-limiting binding of O_2 for the entire series of copper species investigated here. In the case of Cu-tmpa, these potential- and rate-determining steps were already identified on basis of kinetic studies discussed in previous reports.[22,23,62] It is important to note that also the data previously obtained for Cu-bmpa ($E_{1/2}$ = 0.30 V vs RHE, TOF_{max} for ORR = 2.4 × 10^4 s^{-1}) correlates very well with the ORR TOF_{max} versus $E_{1/2}$ trend reported here,[39] while catalysts that show very sluggish and therefore rate-determining Cu(II) reduction kinetics do significantly underperform as one would expect.[39,47,63,64]

Displacement of water for peroxide presumably takes place prior to the rate-determining step of the HPRR, and with similar energetics for all copper complexes, unlike the binding of dioxygen. The relative insensitivity of H_2O_2 versus H_2O binding to these copper sites is to be expected, as both species bind to the copper site in a very similar manner. The actual rate-determining step most likely involves the scission of the O−O bond, presumably via a Fenton-like reaction.[23] This reaction is highly exothermic and occurs far from the equilibrium potential of peroxide ($E^0_{H_2O_2/H_2O}$ = 1.78 V vs RHE) and therefore is expected to be less dependent on the electronic structure of the copper site.

Interestingly, the HPRR and ORR scale differently with $E_{1/2}$ of the catalyst. This implies that the $E_{1/2}$ of the Cu complex must also be a key descriptor regarding the selectivity of the ORR mediated at single site copper species. Our findings from RRDE measurements illustrate that electron-rich copper sites are set up to produce significant amounts of peroxide with fast reaction rates, while electron-poor copper sites will react slower in the ORR and preferably reduce hydrogen peroxide over dioxygen, thus favoring the ultimate formation of water. In practice, it is not always easy to visualize in a single experiment that the ORR selectivity directly correlates to $E_{1/2}$, given that the overall rates of the catalysts are largely different, thereby resulting that these catalysts arrive at a mass transport-limited regime at a different moment. When this is taken into account, a clear correlation between $E_{1/2}$, the ORR and HPRR rates, and the selectivity can be drawn. Catalysts that operate at higher potentials due to a more positive $E_{1/2}$ are expected to reduce dioxygen in an overall 4-electron reduction reaction given that their HPRR rates are significantly larger than the ORR rates, but, in practice, catalytic rates mediated by these species will be sluggish. Consequently, finding a catalyst that can produce hydrogen peroxide selectively near the equilibrium potential of the peroxide will be hard. Catalysts that operate at more negative potentials show a very high affinity for O_2 binding and show very high catalytic rates toward the formation of hydrogen peroxide, yet such catalysts are easily limited by mass transport limitations. When mass transport limitations occur, and locally, most O_2 is consumed, all catalysts are expected to preferentially catalyze the full 4-electron reduction to water.

CONCLUSIONS

We have investigated the correlation between $E_{1/2}$ and the catalytic performance in the oxygen and hydrogen peroxide reduction reactions for a series of copper complexes based on the tetradentate tmpa-based ligand scaffold. Our findings show that the log(TOF_{max}) of the ORR and HPRR correlates linearly with $E_{1/2}$. A direct correlation between the computed O_2 binding constant to $E_{1/2}$ was found as well and is in good agreement with rate-determining binding of O_2 to a Cu^{I} species. Since the ORR and HPRR scale versus $E_{1/2}$ with significantly different slopes, the $E_{1/2}$ value is a leading descriptor for the selectivity of the oxygen reduction process. Our design rules are the following: Copper species with more positive $E_{1/2}$ values are expected to catalyze the overall 4-electron reduction reaction to water more selectively, yet achieving high catalytic rates for such a catalyst will be challenging; catalysts with more negative $E_{1/2}$ values are likely to accumulate hydrogen peroxide, providing that mass transport limitations can be avoided.

ASSOCIATED CONTENT

Supporting Information

The Supporting Information is available free of charge at https://pubs.acs.org/doi/10.1021/acs.inorgchem.3c02939.

Experimental procedures, spectra and crystallographic data, additional voltammetry data and details on determination of the catalytic rate by foot-of-the-wave, current enhancement methods, rotating ring-disk experiments, and computational details (PDF)

Accession Codes

CCDC 2183226 contains the supplementary crystallographic data for this paper. These data can be obtained free of charge via www.ccdc.cam.ac.uk/data_request/cif, or by emailing data_request@ccdc.cam.ac.uk, or by contacting The Cambridge Crystallographic Data Centre, 12 Union Road, Cambridge CB2 1EZ, UK; fax: +44 1223 336033.

AUTHOR INFORMATION

Corresponding Author

Dennis G. H. Hetterscheid − *Leiden Institute of Chemistry, Leiden University, 2300 RA Leiden, The Netherlands;* orcid.org/0000-0001-5640-4416; Email: d.g.h.hetterscheid@chem.leidenuniv.nl

Authors

Michiel Langerman − *Leiden Institute of Chemistry, Leiden University, 2300 RA Leiden, The Netherlands*

Phebe H. van Langevelde − *Leiden Institute of Chemistry, Leiden University, 2300 RA Leiden, The Netherlands*

Johannes J. van de Vijver − *Leiden Institute of Chemistry, Leiden University, 2300 RA Leiden, The Netherlands*

Maxime A. Siegler − *Department of Chemistry, Johns Hopkins University, Baltimore, Maryland 21218, United States;* orcid.org/0000-0003-4165-7810

Complete contact information is available at:

https://doi.org/10.1021/acs.inorgchem.3c02939
Inorg. Chem. 2023, 62, 19593−19602

https://pubs.acs.org/10.1021/acs.inorgchem.3c02939

Notes

The authors declare no competing financial interest.

■ ACKNOWLEDGMENTS

Financial support was provided by the European Research Council (ERC starting grant 637556 and ERC proof-of-concept grant 899535 to D.G.H. Hetterscheid).

■ REFERENCES

(1) An, L.; Zhao, T. S.; Zhou, X. L.; Wei, L.; Yan, X. H. A high-performance ethanol-hydrogen peroxide fuel cell. *RSC Adv.* **2014**, *4* (110), 65031−65034.
(2) Cano, Z. P.; Banham, D.; Ye, S. Y.; Hintennach, A.; Lu, J.; Fowler, M.; Chen, Z. W. Batteries and fuel cells for emerging electric vehicle markets. *Nat. Energy* **2018**, *3* (4), 279−289.
(3) Fukuzumi, S.; Yamada, Y.; Karlin, K. D. Hydrogen peroxide as a sustainable energy carrier: Electrocatalytic production of hydrogen peroxide and the fuel cell. *Electrochim. Acta* **2012**, *82*, 493−511.
(4) Gasteiger, H. A.; Kocha, S. S.; Sompalli, B.; Wagner, F. T. Activity benchmarks and requirements for Pt, Pt-alloy, and non-Pt oxygen reduction catalysts for PEMFCs. *Appl. Catal., B* **2005**, *56* (1−2), 9−35.
(5) Grigoropoulou, G.; Clark, J. H.; Elings, J. A. Recent developments on the epoxidation of alkenes using hydrogen peroxide as an oxidant. *Green Chem.* **2003**, *5* (1), 1−7.
(6) Gröger, O.; Gasteiger, H. A.; Suchsland, J. P. Review-Electromobility: Batteries or Fuel Cells? *J. Electrochem. Soc.* **2015**, *162* (14), A2605−A2622.
(7) Zeronian, S. H.; Inglesby, M. K. Bleaching of cellulose by hydrogen peroxide. *Cellulose* **1995**, *2* (4), 265−272.
(8) Solomon, E. I.; Heppner, D. E.; Johnston, E. M.; Ginsbach, J. W.; Cirera, J.; Qayyum, M.; Kieber-Emmons, M. T.; Kjaergaard, C. H.; Hadt, R. G.; Tian, L. Copper Active Sites in Biology. *Chem. Rev.* **2014**, *114* (7), 3659−3853.
(9) Rolff, M.; Schottenheim, J.; Decker, H.; Tuczek, F. Copper-O_2 reactivity of tyrosinase models towards external monophenolic substrates: molecular mechanism and comparison with the enzyme. *Chem. Soc. Rev.* **2011**, *40* (7), 4077−4098.
(10) Elwell, C. E.; Gagnon, N. L.; Neisen, B. D.; Dhar, D.; Spaeth, A. D.; Yee, G. M.; Tolman, W. B. Copper-Oxygen Complexes Revisited: Structures, Spectroscopy, and Reactivity. *Chem. Rev.* **2017**, *117* (3), 2059−2107.
(11) Mirica, L. M.; Ottenwaelder, X.; Stack, T. D. P. Structure and spectroscopy of copper-dioxygen complexes. *Chem. Rev.* **2004**, *104* (2), 1013−1045.
(12) Hong, S.; Lee, Y. M.; Ray, K.; Nam, W. Dioxygen activation chemistry by synthetic mononuclear nonheme iron, copper and chromium complexes. *Coord. Chem. Rev.* **2017**, *334*, 25−42.
(13) Halfen, J. A.; Mahapatra, S.; Wilkinson, E. C.; Kaderli, S.; Young, V. G., Jr.; Que, L., Jr.; Zuberbuhler, A. D.; Tolman, W. B. Reversible cleavage and formation of the dioxygen O-O bond within a dicopper complex. *Science* **1996**, *271* (5254), 1397−400.
(14) Shimoyama, Y.; Kojima, T. Metal-Oxyl Species and Their Possible Roles in Chemical Oxidations. *Inorg. Chem.* **2019**, *58* (15), 9517−9542.
(15) Lee, J. Y.; Kim, S.; Cowley, R.; Ginsbach, J.; Siegler, M.; Solomon, E.; Karlin, K. Evolution of Thioether S-ligated Primary Cu^I/O_2 Adducts: The 1st Example of CuII-Superoxo Species with Enhanced Reactivity. In *Abstracts of Papers of the American Chemical Society*; American Chemical Society, 2015; Vol. *249*.
(16) Diaz, D. E.; Quist, D. A.; Herzog, A. E.; Schaefer, A. W.; Kipouros, I.; Bhadra, M.; Solomon, E. I.; Karlin, K. D. Impact of Intramolecular Hydrogen Bonding on the Reactivity of Cupric Superoxide Complexes with O-H and C-H Substrates. *Angew. Chem., Int. Ed.* **2019**, *58* (49), 17572−17576.
(17) Kim, B.; Jeong, D.; Ohta, T.; Cho, J. Nucleophilic reactivity of a copper(II)-hydroperoxo complex. *Commun. Chem.* **2019**, *2*, No. 81, DOI: 10.1038/s42004-019-0187-3.
(18) Collman, J. P.; Devaraj, N. K.; Decreau, R. A.; Yang, Y.; Yan, Y. L.; Ebina, W.; Eberspacher, T. A.; Chidsey, C. E. D. A cytochrome c oxidase model catalyzes oxygen to water reduction under rate-limiting electron flux. *Science* **2007**, *315* (5818), 1565−1568.
(19) van Dijk, B.; Hofmann, J. P.; Hetterscheid, D. G. H. Pinpointing the active species of the Cu(DAT) catalyzed oxygen reduction reaction. *Phys. Chem. Chem. Phys.* **2018**, *20* (29), 19625−19634.
(20) Thorum, M. S.; Yadav, J.; Gewirth, A. A. Oxygen Reduction Activity of a Copper Complex of 3,5-Diamino-1,2,4-triazole Supported on Carbon Black. *Angew. Chem., Int. Ed.* **2009**, *48* (1), 165−167.
(21) Muñoz-Becerra, K.; Zagal, J. H.; Venegas, R.; Recio, F. J. Strategies to improve the catalytic activity and stability of bioinspired Cu molecular catalysts for the ORR. *Curr. Opin. Electrochem.* **2022**, *35*, No. 101035, DOI: 10.1016/j.coelec.2022.101035.
(22) Langerman, M.; Hetterscheid, D. G. H. Fast Oxygen Reduction Catalyzed by a Copper(II) Tris(2-pyridylmethyl)amine Complex through a Stepwise Mechanism. *Angew. Chem., Int. Ed.* **2019**, *58* (37), 12974−12978.
(23) Langerman, M.; Hetterscheid, D. G. H. Mechanistic Study of the Activation and the Electrocatalytic Reduction of Hydrogen Peroxide by Cu-tmpa in Neutral Aqueous Solution. *ChemElectroChem* **2021**, *8* (15), 2783−2791.
(24) Langerman, M.; van Dorth, M.; Hetterscheid, D. G. H. Dioxygen reduction in acetonitrile with copper pyridylalkylamine complexes: The influence of acid strength on the catalytic performance. *Eur. J. Inorg. Chem.* **2023**, *26*, No. e202300218.25.
(25) Karlin, K. D.; Hayes, J. C.; Juen, S.; Hutchinson, J. P.; Zubieta, J. Tetragonal Vs Trigonal Coordination in Copper(II) Complexes with Tripod Ligands—Structures and Properties of $[Cu(C_{21}H_{24}N_4)Cl]PF_6$ and $[Cu(C_{18}H_{18}N_4)Cl]PF_6$. *Inorg. Chem.* **1982**, *21* (11), 4106−4108.
(26) Ambundo, E. A.; Deydier, M. V.; Grall, A. J.; Aguera-Vega, N.; Dressel, L. T.; Cooper, T. H.; Heeg, M. J.; Ochrymowycz, L. A.; Rorabacher, D. B. Influence of coordination geometry upon copper(II/I) redox potentials. Physical parameters for twelve copper tripodal ligand complexes. *Inorg. Chem.* **1999**, *38* (19), 4233−4242.
(27) Schatz, M.; Becker, M.; Thaler, F.; Hampel, F.; Schindler, S.; Jacobson, R. R.; Tyeklar, Z.; Murthy, N. N.; Ghosh, P.; Chen, Q.; Zubieta, J.; Karlin, K. D. Copper(I) complexes, copper(I)/O_2 reactivity, and copper(II) complex adducts, with a series of tetradentate tripyridylalkylamine tripodal ligands. *Inorg. Chem.* **2001**, *40* (10), 2312−2322.
(28) Foxon, S. P.; Walter, O.; Schindler, S. Syntheses and characterization of copper(II) complexes of the new Ligands N-[(2-pyridyl)methyl]-2,2′-dipyridylamine and N-[Bis(2-pyridyl)methyl]-2-pyridylamine. *Eur. J. Inorg. Chem.* **2002**, *2002* (1), 111−121.
(29) Fujii, T.; Naito, A.; Yamaguchi, S.; Wada, A.; Funahashi, Y.; Jitsukawa, K.; Nagatomo, S.; Kitagawa, T.; Masuda, H. Construction of a square-planar hydroperoxo-copper(II) complex inducing a higher catalytic reactivity. *Chem. Commun.* **2003**, *21*, 2700−2701.
(30) Das, D.; Lee, Y. M.; Ohkubo, K.; Nam, W.; Karlin, K. D.; Fukuzumi, S. Temperature-Independent Catalytic Two-Electron Reduction of Dioxygen by Ferrocenes with a Copper(II) Tris[2-(2-pyridyl)ethyl]amine Catalyst in the Presence of Perchloric Acid. *J. Am. Chem. Soc.* **2013**, *135* (7), 2825−2834.
(31) Addison, A. W. Is Ligand Topology an Influence on the Redox Potentials of Copper-Complexes. *Inorg. Chim. Acta* **1989**, *162* (2), 217−220.
(32) Nagao, H.; Komeda, N.; Mukaida, M.; Suzuki, M.; Tanaka, K. Structural and electrochemical comparison of copper(II) complexes with tripodal ligands. *Inorg. Chem.* **1996**, *35* (23), 6809−6815.
(33) Patterson, G. S.; Holm, R. H. Structural and electronic effects on the polarographic half-wave potentials of copper (II) chelate complexes. *Bioinorg. Chem.* **1975**, *4* (3), 257−275.

(34) Lucas, H. R.; Meyer, G. J.; Karlin, K. D. CO and O_2 Binding to Pseudo-tetradentate Ligand-Copper(I) Complexes with a Variable N-Donor Moiety: Kinetic/Thermodynamic Investigation Reveals Ligand-Induced Changes in Reaction Mechanism. *J. Am. Chem. Soc.* **2010**, *132* (37), 12927−12940.
(35) Lee, Y.; Park, G. Y.; Lucas, H. R.; Vajda, P. L.; Kamaraj, K.; Vance, M. A.; Milligan, A. E.; Woertink, J. S.; Siegler, M. A.; Sarjeant, A. A. N.; Zakharov, L. N.; Rheingold, A. L.; Solomon, E. I.; Karlin, K. D. Copper(I)/O(2)Chemistry with Imidazole Containing Tripodal Tetradentate Ligands Leading to mu-1,2-Peroxo-Dicopper(II) Species. *Inorg. Chem.* **2009**, *48* (23), 11297−11309.
(36) Kakuda, S.; Peterson, R. L.; Ohkubo, K.; Karlin, K. D.; Fukuzumi, S. Enhanced Catalytic Four-Electron Dioxygen (O_2) and Two-Electron Hydrogen Peroxide (H_2O_2) Reduction with a Copper-(II) Complex Possessing a Pendant Ligand Pivalamido Group. *J. Am. Chem. Soc.* **2013**, *135* (17), 6513−6522.
(37) Drover, M. W. A guide to secondary coordination sphere editing. *Chem. Soc. Rev.* **2022**, *51* (6), 1861−1880.
(38) Sinha, S.; Williams, C. K.; Jiang, J. Outer-coordination sphere in multi-H^+/multi-e(-) molecular electrocatalysis. *Iscience* **2022**, *25* (1), No. 103628, DOI: 10.1016/j.isci.2021.103628.
(39) Smits, N. W. G.; van Dijk, B.; de Bruin, I.; Groeneveld, S. L. T.; Siegler, M. A.; Hetterscheid, D. G. H. Influence of Ligand Denticity and Flexibility on the Molecular Copper Mediated Oxygen Reduction Reaction. *Inorg. Chem.* **2020**, *59* (22), 16398−16409.
(40) Lonnon, D. G.; Craig, D. C.; Colbran, S. B. Rhodium, palladium and platinum complexes of tris(pyridylalkyl)amine and tris(benzimidazolylmethyl)amine N_4-tripodal ligands. *Dalton Trans.* **2006**, No. 31, 3785−3797.
(41) Hathaway, B. J.; Hodgson, P. G. Copper-Ligand Bond-Lengths in Axial Complexes of Copper(II) Ion. *J. Inorg. Nucl. Chem.* **1973**, *35* (12), 4071−4081.
(42) De Almeida, K. J.; Murugan, N. A.; Rinkevicius, Z.; Hugosson, H. W.; Vahtras, O.; Agren, H.; Cesar, A. Conformations, structural transitions and visible near-infrared absorption spectra of four-, five- and six-coordinated Cu(II) aqua complexes. *Phys. Chem. Chem. Phys.* **2009**, *11* (3), 508−519.
(43) See, R. F.; Kruse, R. A.; Strub, W. M. Metal-ligand bond distances in first-row transition metal coordination compounds: Coordination number, oxidation state, and specific ligand effects. *Inorg. Chem.* **1998**, *37* (20), 5369−5375.
(44) Nimmermark, A.; Ohrstrom, L.; Reedijk, J. Metal-ligand bond lengths and strengths: are they correlated? A detailed CSD analysis. *Z. Krist-Cryst. Mater.* **2013**, *228* (7), 311−317.
(45) Hall, S. B.; Khudaisha, E. A.; Hart, A. L. Electrochemical oxidation of hydrogen peroxide at platinum electrodes. Part III: Effect of temperature. *Electrochim. Acta* **1999**, *44*, 2455−2462.
(46) Van Stroe-Biezen, S. A. M.; Everaerts, F. M.; Janssen, L. J. J.; Tacken, R. A. Diffusion coefficients of oxygen, hydrogen peroxide and glucose in a hydrogel. *Anal. Chim. Acta* **1993**, *273*, 553−560.
(47) Smits, N. W. G.; Rademaker, D.; Konovalov, A. I.; Siegler, M. A.; Hetterscheid, D. G. H. Influence of the spatial distribution of copper sites on the selectivity of the oxygen reduction reaction. *Dalton Trans.* **2022**, *51* (3), 1206−1215.
(48) Van Dijk, B.; Kinders, R.; Ferber, T. H.; Hofmann, J. P.; Hetterscheid, D. G. H. A Selective Copper BAsed Oxygen Reduction Catalyst for the Electrochemical Synthesis of H_2O_2 at Neutral pH. *ChemElectroChem* **2022**, *9*, No. e202101692.
(49) Rountree, E. S.; McCarthy, B. D.; Eisenhart, T. T.; Dempsey, J. L. Evaluation of Homogeneous Electrocatalysts by Cyclic Voltammetry. *Inorg. Chem.* **2014**, *53* (19), 9983−10002.
(50) Xing, W.; Lv, M.; Hu, Y.; Liu, C.; Zhang, J. Oxygen Solubility, Diffusion Coefficient, and Solution Viscosity. In *Rotating Electrode Methods and Oxygen Reduction Electrocatalysts*; Elsevier, 2014; Chapter 1, pp 1−31.
(51) Martin, D. J.; Mercado, B. Q.; Mayer, J. M. Combining scaling relationships overcomes rate versus overpotential trade-offs in O_2 molecular electrocatalysis. *Sci. Adv.* **2020**, *6* (11), No. eaaz3318.
(52) Wang, V. C.-C.; Johnson, B. A. Interpreting the Electrocatalytic Voltammetry of Homogeneous Catalysts by the Foot of the Wave Analysis and Its Wider Implications. *ACS Catal.* **2019**, *9* (8), 7109−7123.
(53) Ginsbach, J. W.; Peterson, R. L.; Cowley, R. E.; Karlin, K. D.; Solomon, E. I. Correlation of the Electronic and Geometric Structures in Mononuclear Copper(II) Superoxide Complexes. *Inorg. Chem.* **2013**, *52* (22), 12872−12874.
(54) Peterson, R. L.; Himes, R. A.; Kotani, H.; Suenobu, T.; Tian, L.; Siegler, M. A.; Solomon, E. I.; Fukuzumi, S.; Karlin, K. D. Cupric Superoxo-Mediated Intermolecular C-H Activation Chemistry. *J. Am. Chem. Soc.* **2011**, *133* (6), 1702−1705.
(55) Rorabacher, D. B. Electron transfer by copper centers. *Chem. Rev.* **2004**, *104* (2), 651−697.
(56) Krylova, K.; Jackson, K. D.; Vroman, J. A.; Grall, A. J.; Snow, M. R.; Ochrymowycz, L. A.; Rorabacher, D. B. Ring size, substituent, and anion effects on the kinetic and equilibrium properties of copper(II) complexes with water-soluble macrocyclic tetrathia ethers. *Inorg. Chem.* **1997**, *36* (27), 6216−6223.
(57) Shaw, W. J.; Helm, M. L.; DuBois, D. L. A modular, energy-based approach to the development of nickel containing molecular electrocatalysts for hydrogen production and oxidation. *Biochim. Biophys. Acta, Bioenerg.* **2013**, *1827* (8−9), 1123−1139.
(58) Pegis, M. L.; McKeown, B. A.; Kumar, N.; Lang, K.; Wasylenko, D. J.; Zhang, X. P.; Raugei, S.; Mayer, J. M. Homogenous Electrocatalytic Oxygen Reduction Rates Correlate with Reaction Overpotential in Acidic Organic Solutions. *ACS Cent. Sci.* **2016**, *2* (11), 850−856.
(59) Wang, Y. H.; Pegis, M. L.; Mayer, J. M.; Stahl, S. S. Molecular Cobalt Catalysts for O_2 Reduction: Low-Overpotential Production of H_2O_2 and Comparison with Iron-Based Catalysts. *J. Am. Chem. Soc.* **2017**, *139* (46), 16458−16461.
(60) Pegis, M. L.; Wise, C. F.; Koronkiewicz, B.; Mayer, J. M. Identifying and Breaking Scaling Relations in Molecular Catalysis of Electrochemical Reactions. *J. Am. Chem. Soc.* **2017**, *139* (32), 11000−11003.
(61) Klug, C. M.; Cardenas, A. J. P.; Bullock, R. M.; O'Hagan, M.; Wiedner, E. S. Reversing the Tradeoff between Rate and Overpotential in Molecular Electrocatalysts for H-2 Production. *ACS Catal.* **2018**, *8* (4), 3286−3296.
(62) Fry, H. C.; Scaltrito, D. V.; Karlin, K. D.; Meyer, G. J. The rate of O_2 and CO binding to a copper complex, determined by a "flash-and-trap" technique, exceeds that for hemes. *J. Am. Chem. Soc.* **2003**, *125* (39), 11866−11871.
(63) Van Langevelde, P. H.; Kounalis, E.; Killian, L.; Monkcom, E. C.; Broere, D. L. J.; Hetterscheid, D. G. H. Mechanistic Investigations into the Selective Reduction of Oxygen by a Multicopper Oxidase T3 Site-Inspired Dicopper Complex. *ACS Catal.* **2023**, *13* (8), 5712−5722.
(64) Budhija, V.; van Langevelde, P. H.; Krause, K. B.; Cula, B.; Hetterscheid, D. G. H.; Schwalbe, M. Synthesis, Properties and Reactivity Studies of a Hetero-dicopper Complex Consisting of a Porphyrin and a Bispyridylamine Moiety Connected by a Xanthene Backbone. *Eur. J. Inorg. Chem.* **2023**, *26* (14), No. e202200743, DOI: 10.1002/ejic.202200743.